



HAL
open science

Molecular Functionalization of Chemically Active Defects in WSe₂ for Enhanced Opto-Electronics

Yuda Zhao, Sai Manoj Gali, Can Wang, Anton Pershin, Amine Slassi, David Beljonne, Paolo Samori

► **To cite this version:**

Yuda Zhao, Sai Manoj Gali, Can Wang, Anton Pershin, Amine Slassi, et al.. Molecular Functionalization of Chemically Active Defects in WSe₂ for Enhanced Opto-Electronics. *Advanced Functional Materials*, 2020, 30 (45), pp.2005045. 10.1002/adfm.202005045 . hal-03017538

HAL Id: hal-03017538

<https://hal.science/hal-03017538v1>

Submitted on 20 Nov 2020

HAL is a multi-disciplinary open access archive for the deposit and dissemination of scientific research documents, whether they are published or not. The documents may come from teaching and research institutions in France or abroad, or from public or private research centers.

L'archive ouverte pluridisciplinaire **HAL**, est destinée au dépôt et à la diffusion de documents scientifiques de niveau recherche, publiés ou non, émanant des établissements d'enseignement et de recherche français ou étrangers, des laboratoires publics ou privés.

Molecular Functionalization of Chemically Active Defects in WSe₂ for Enhanced Optoelectronics

*Yuda Zhao, Sai Manoj Gali, Can Wang, Anton Pershin, Amine Slassi, David Beljonne, Paolo Samorì**

Dr. Y. Zhao, Dr. C. Wang, Prof. P. Samorì
University of Strasbourg, CNRS, ISIS UMR 7006, 8 allée Gaspard Monge, F-67000
Strasbourg, France
E-mail: samori@unistra.fr

Dr. S. M. Gali, Dr. A. Pershin,^[+] Dr. A. Slassi, Prof. D. Beljonne
Laboratory for Chemistry of Novel Materials, University of Mons, 7000-Mons, Belgium

^[+]Presnet address: Wigner Research Centre for Physics, PO Box 49, H-1525 Budapest, Hungary

Keywords: transition metal dichalcogenides, vacancy defect, thiol chemistry, field-effect transistor, photoluminescence

Structural defects are known to worsen electrical and optical properties of two-dimensional (2D) materials. Transition metal dichalcogenides (TMDs) are prone to chalcogen vacancies and molecular functionalization of these vacancies offers a powerful strategy to engineer the crystal structure by healing such defects. This molecular approach can effectively improve physical properties of 2D materials and optimize the performance of 2D electronic devices. While this strategy has been successfully exploited to heal vacancies in sulfides, its viability on selenides based TMDs has not yet been proven. Here, by using thiophenol molecules to functionalize monolayer WSe₂ surface containing Se vacancies, we demonstrate that the defect healing via molecular approach not only improves the performance of WSe₂ transistors (>10-fold increase in the current density, the electron mobility, and the I_{on}/I_{off} ratio), but also enhances the photoluminescence properties of monolayer WSe₂ flakes (three-fold increase of PL intensity at room temperature). Theoretical calculations elucidate the mechanism of molecular passivation, which originates from the strong interaction between thiol functional group at Se vacancy sites and neighboring tungsten atoms. These results demonstrate that our molecular approach

represents a powerful strategy to engineer WSe₂ FETs and optimize their optical properties, paving the way towards high-performance 2D (opto)electronic devices.

1. Introduction

Atomically thick two-dimensional materials display numerous outstanding physical and chemical properties. In particular, their high immunity to short-channel effects have shown promising applications in next-generation field-effect transistors (FETs).^[1-3] The star 2D semiconductor, i.e. MoS₂, exhibits high electron mobility ranging from 10 to >100 cm²V⁻¹s⁻¹ at room temperature and large I_{on}/I_{off} current ratio (>10⁵),^[4-6] thereby outperforming Si transistors with similar channel thickness.^[7] Compared with the extensively studied MoS₂ devices, the transport behavior of monolayer WSe₂ FETs shows stronger dependence on the contact metal and the surrounding dielectric environment, exhibiting different transport modes (unipolar/ambipolar) and varying dominant carriers (electron/hole).^[8-10] In addition, large discrepancies of carrier mobility in 2D transistors between theoretical predictions and experimental results can be found in literature.^[11-14] These all inspire researchers to study the impact of intrinsic and extrinsic defects in 2D materials on their charge transport properties in transistors.^[15]

The main type of intrinsic defects in monolayer MoS₂ prepared by mechanical exfoliation method using scotch tape and chemical vapor deposition (CVD) method has been identified as sulfur vacancies.^[16-18] The concentration of single sulfur vacancy has been estimated at over 1×10^{13} cm⁻² in monolayer mechanical exfoliated samples.^[19] This number can reach 8.6×10^{13} cm⁻² in monolayer CVD samples, which corresponds to 3% of S content in MoS₂.^[20] These vacancies induce localized defect states and result in the hopping transport of charge carriers in 2D layers.^[21]

The molecular approach has been widely exploited to functionalize 2D materials.^[22, 23] The healing of sulfur vacancies in monolayer MoS₂ FET with thiolated molecules yielded improved

performance with band-like transport behavior and the electron mobility as high as $150 \text{ cm}^2 \text{V}^{-1} \text{s}^{-1}$.^[24-26] On the same time, the passivation of defects can dramatically improve the optical properties of 2D layers, for example reaching photoluminescence quantum yields in MoS_2 approaching the unity.^[27] Therefore, it is of vital importance to study the intrinsic defects in WSe_2 , analyze the correlation between the defects and the physical properties of WSe_2 , and finally explore the molecular methods to passivate the defects in order to improve optical properties and device performance.

In our work, thiophenol molecules are functionalized on intrinsic Se vacancies of WSe_2 samples, which has been directly identified by scanning tunneling microscope (STM) imaging for the first time. The improved charge transport in monolayer WSe_2 back-gate FETs and the efficient photoluminescence (PL) emission of monolayer flake after thiophenol functionalization experimentally demonstrate the successful defect passivation via the molecular approach. WSe_2 FET show an over 10-fold increase in the current density, the electron mobility, and the $I_{\text{on}}/I_{\text{off}}$ ratio. Theoretical calculations indicate that a strong interaction of thiol functional group with Se vacancies in WSe_2 determines the elimination of defect states and the shift of work function via n-type doping effect. Our combined experimental and theoretical research represents a viable route to engineer defects in the monolayer WSe_2 towards high-performance transistors and high-efficiency photoluminescence materials.

2. Results and Discussion

Intrinsic defects in WSe_2 are firstly identified by STM imaging in ambient conditions on a freshly mechanically exfoliated surface of WSe_2 crystals. Figure 1a and Figure S1 show the atomic resolution STM height image of WSe_2 . It displays a lattice constant of $a = b = 0.33 \text{ nm}$ and $\gamma = 120^\circ$, in good accordance with theoretical lattice parameters. Some point-like defects (dark circular feature in the STM image) are observed in the two-dimensional Se atom arrays. Theoretical calculations reveal that from an energetic viewpoint, the energy required to form

Se vacancies, exposed in the outer surface, is lower compared to the generation of vacancies of W, which are embedded in the underlying layer.^[28, 29] We infer that the defects observed in the STM image are most likely Se vacancies, and the simulated STM image showing the surface electron state of WSe₂ with 0.7% Se vacancy in Figure 1b further confirms our interpretation. The strong brightness difference between W and Se atoms indicate the electron rich nature in the Se sites on the crystal surface, and the missing of one bright dot refers to a Se vacancy site. Molecules with hydroxyl, thiol or selenol functional groups are promising candidates to passivate Se vacancies in monolayer WSe₂. Considering of the steric effect in Se vacancy sites, molecules with thiol or selenol functional group are more suitable for passivating single-point Se vacancies. Compared with thiolated molecules, selenol molecules can be easily oxidized and their thermal stability is quite poor,^[30] as also demonstrated by our device characterizations in the latter sections. Therefore, in this work we mainly focus our attention on the use of thiolated molecules, i.e. thiophenol (abbreviated to PhSH in the figures) to repair Se vacancies on WSe₂ surface. We implemented a vapor-phase deposition method to exclude the contribution from solvents in the common solution processing.^[31] Specifically, the thiophenol molecules are heated in a sealed bottle with WSe₂ samples directly exposed to the molecular vapors. After the molecular adsorption, the WSe₂ surface was immediately covered with a drop of 1-phenyloctane and characterized by STM at the liquid/solid interface. The high-resolution image in Figure 1c shows a bright dot, which can be ascribed to an adsorbed thiophenol molecule filling the Se vacancy. The weakly bonded physisorbed thiophenol molecules have been dissolved in 1-phenyloctane, thus has desorbed from the WSe₂. Hence, they cannot be visualized under our scanning condition. The adsorption configuration of a thiophenol molecule on the single Se vacancy site was confirmed by the comparison between theoretical simulations and experimental STM images. Two possible adsorption configurations are selected including the vertical (benzene ring arranged perpendicular to the 2D basal plane, Figure S2a) and horizontal (benzene ring lying flat and parallel to the 2D basal plane, Figure S2b) packing of thiophenol

on WSe₂ surface. By comparing the calculated adsorption energy at the two configurations (vertical: -0.83 eV and horizontal: -0.60 eV), we conclude that thiophenol molecules are prone to adsorb vertically at the Se vacancy site. The simulated STM images of the adsorbed thiophenol molecule at the vertical stacking configuration (Figure 1d) is consistent with the experimental STM images (Figure 1c). By gradually decreasing the tip-sample distance, the STM tip could reach the position under the phenyl group of thiophenol. As seen in Figure S3, the underneath Se atom arrays become clear with no point defect, while the bright dots referred to thiophenol are still observable. This set of STM images can also demonstrate the vertical stacking configuration of thiophenol on WSe₂ surface. Meanwhile, these vertically adsorbed molecules are quite stably attached to the Se vacancy points.

After the successful demonstration of thiophenol functionalization on Se vacancy sites in WSe₂ by the STM characterization, it is very important to explore the effect of defect passivation on the material properties and the FET performance. The scheme of the FET device architectures is portrayed in Figure 2a. A back-gate monolayer WSe₂ FET was fabricated on the SiO₂/Si substrate with Au metal electrodes. After device fabrication, a vacuum annealing process was performed in order to remove the surface contamination and expose the vacancy sites. Then thiophenol molecules were functionalized on the monolayer WSe₂ surface to passivate Se vacancies. The effect induced by molecules on the transfer characteristics of WSe₂ FET is displayed in Figure 2b. The molecular functionalization increases the on-current level, improves the field-effect mobility (from 0.015 to 0.025 cm²V⁻¹s⁻¹), and enhances the I_{on}/I_{off} ratio (from 1 × 10⁴ to 3 × 10⁴). In order to increase the density of strongly grafted molecules, a second vacuum annealing process was conducted to enhance the interaction between molecules and vacancy sites. Compared with the pristine WSe₂ devices, the annealing process induces the increase of the drain current at V_g = 90 V by almost two orders of magnitude, the improvement of electron mobility from 0.015 to 0.79 cm²V⁻¹s⁻¹, and the enhancement of the I_{on}/I_{off} ratio from 1 × 10⁴ to 1 × 10⁶. The shift of threshold voltage extracted from the transfer curves shows the

increase of electron density by $1.04 \times 10^{12} \text{ cm}^{-2}$, exhibiting the n-type doping induced by the thiophenol molecules. The output curves (Figure S4a) of pristine WSe₂ FET show a superlinear relationship within 1.5 V drain biases, demonstrating a relatively large contact resistance. The molecular functionalization results in a less superlinear output curves (Figure S4b) due to the increased electron density and the decreased contact resistance. Atomic force microscopy (AFM) imaging (Figure S5) was used to monitor the morphology change of WSe₂ surface before and after the second annealing process, providing unambiguous evidence for the removal of weakly physisorbed molecules. Therefore, the strongly adsorbed thiophenol molecules on the Se vacancy sites induce n-type doping on the channel region and greatly improve the FET performance.

The optical property of monolayer WSe₂, i.e. PL spectrum, is known to be very sensitive to the defect states.^[32, 33] Therefore, we further studied the effect of thiophenol functionalization on PL spectra. The room-temperature PL spectra of monolayer WSe₂ (inset of Figure 2c) displays a broad peak centered at 1.63 eV; the chemical functionalization with thiophenol molecules increases the PL intensity of WSe₂ by a factor of 2.6. As the temperature decreases, electron-phonon scattering becomes weak and PL peaks from localized exciton emissions can be more pronounced. The broad PL peak at 77 K (Figure 2c) can be fitted into three peaks in Figure 2d, including one defect-related peak (X_b at 1.61 eV) and two negatively charged trion peaks (X^- at 1.68 eV and X'^- at 1.66 eV).^[33] The X_b peak originates from the excitons bound to defects, which can act as an indicator for defects in WSe₂.^[15] The negatively charged trion peaks are attributed to the emission from a localized excitation which consists of three charged particles (two electrons and one hole). The thiophenol molecules and the subsequent annealing process together decrease the spectral weight of X_b peak and increase the spectral weight of X'^- peak, demonstrating the successful defect passivation and n-type doping effect.

X-ray photoelectron spectroscopy (XPS) was used to further verify the doping effect from molecules. Figure S6 compares the binding energies for the W 4f_{5/2}, W 4f_{7/2}, Se 3d_{3/2}, and Se

$3d_{5/2}$ peaks before and after molecular functionalization. The binding energies of two W 4f peaks and two Se 3d peaks are shifted upward by 0.4 eV and 0.5 eV, respectively. It indicates a shift of the Fermi level towards the conduction band. Therefore, XPS characterizations confirm the n-type doping on WSe₂ by thiophenol molecules, which is consistent with PL results.

Theoretical calculations were used to study the defect passivation mechanism. Figure 3a shows the electronic band structure of monolayer WSe₂ (4×4 supercell) with single Se vacancy (3% Se vacancy concentration, hitherto referred to as WSe₂ (-3% Se)) calculated using density functional theory (DFT). The Se vacancies introduce midgap defect states below the intrinsic conduction band minimum (CBM) at K point by 0.13 eV and 0.18 eV. These relatively deep defect-related localized states should act as traps and limit the electronic charge transport, while simultaneously creating new defect-related optical emission peaks. It explains the inferior performance of FET based on as-prepared WSe₂, with low current density and low electron density (Figure 2b). Furthermore, the defect-related PL peak X_b (Figure 2d) has been observed at 1.61 eV, which is 0.12 eV smaller than the exciton PL peak X₀ at 1.73 eV,^[33] in very good agreement with theoretical prediction of the energy levels of midgap defect states.

The calculated electronic band structure of monolayer WSe₂ with thiophenol passivation shows two possible configurations, as presented in Figure 3b and 3c. While the midgap defect states originating from the Se vacancy were partially recovered in Figure 3b, they are completely recovered in Figure 3c. The atomic configurations pertaining to Figure 3b and 3c were extracted at different time steps along *ab initio* molecular dynamics (ab-MD) simulations (Figure S7) and differ in the relative positioning of thiol group with respect to the three neighboring tungsten atoms in the vicinity of Se vacancy. As indicated in the inset of Figure 3c, if the sulfur (hydrogen) atom is close to two (one) of the three neighboring tungsten atoms (by ≤ 2.7 Å), a complete recovery of the localized midgap defect states is observed. However, if the sulfur (hydrogen) atom is close to one (two) of the neighboring tungsten atoms, as indicated in the

inset of Figure 3b, only a partial recovery of the midgap defect states is observed. This interaction strength between the thiol group and the neighboring tungsten atoms at the Se vacancy site, is further quantified by DDEC6 calculations with specific analysis on bond orders and overlap populations (see Table S1 for details). A non-zero bond order exists between thiol group with neighboring W atoms, which is also responsible for the stability of thiophenol molecule vertically stacked atop Se vacancy. For the atomic and electronic configuration pertaining to Figure 3c (full recovery of midgap defect states), the bond order (overlap population) of sulfur atom with two neighboring tungsten atoms (highlighted in red color in the inset of Figure 3c) is ≥ 0.55 (≥ 0.42), whereas that of hydrogen atom with the remaining tungsten atom (highlighted in blue color in the inset of Figure 3c) is ≈ 0.7 (≈ 0.5). On the other hand, for the atomic and electronic configurations in Figure 3b, the bond order (overlap population) of sulfur atom with two neighboring tungsten atoms (highlighted in blue color in the inset of Figure 3b) is ≤ 0.11 (≈ 0.1), whereas that of hydrogen atom with the same two tungsten atoms is ≥ 0.46 (≥ 0.35). For all configurations, the sulfur atom is always connected to the carbon atom (S-C) of the molecule, with a strong covalent character (bond order ≥ 1.0). The main message that ensues from this analysis is that the healing of the midgap electronic states is a dynamic effect, with switching back and forth between configurations like those in Figures 3b and 3c taking place over picosecond timescales. Therefore, it follows that an electron trapped at a given time might be released shortly after when thiolated molecules adopt a more favorable configuration in the vicinity of the Se vacancy. In addition, the calculated work function of pristine and functionalized WSe₂ (E_f^{BG} in Table S2) is 4.31 eV and 4.10 eV, respectively. The shift in work function by 0.21 eV, which mostly originates from the axial dipole component of thiophenol molecules, is thus consistent with n-type doping by the molecules. The charge density difference plot of WSe₂ with thiophenol in Figure 3d, calculated as the difference between the total charge density of thiophenol adsorbed on WSe₂ (-3% Se) and the combined charge density of isolated thiophenol molecule and the WSe₂ (-3% Se),

shows a very strong interaction between the WSe₂ (−3% Se) surface with thiophenol at the Se vacancy site.

In contrast, our theoretical calculations (Table S2) show that the stacking of thiophenol molecules on the vacancy-free WSe₂ surface and on oxygen passivated Se vacancy can hardly change the work function of WSe₂ layer. Therefore, it is desirable to find a remote control, such as an external stimulus, to increase the reactivity of the WSe₂. This defect engineering process can be instrumental towards an improved functionalization of the WSe₂ layer with thiophenol molecules to modulate the carrier density of WSe₂. We explore the use of a mild etching strategy, i.e. laser irradiation, to expose and create more vacancy sites. A focused laser beam with a relatively high power density $2.6 \times 10^5 \text{ W/cm}^2$ enables to raise the local temperature, promoting the desorption of molecules physisorbed on the WSe₂ surface and even surpasses the decomposition temperature of WSe₂.^[34] After 6 min laser irradiation, the transfer curves in Figure 4a show that the drain current of WSe₂ FET at $V_g = 80 \text{ V}$ decreased by a factor of 4. The thiophenol functionalization and the following annealing process recovered the drain current and even exceeded the pristine value. Compared with pristine FET device, the drain current, the electron mobility, and the $I_{\text{on}}/I_{\text{off}}$ ratio increased by a factor of 10. The transfer curves with different V_g sweep directions in Figure 4b display the change of hysteresis before and after molecular functionalization. Compared with pristine devices, the hysteresis in the thiophenol passivated devices at $I_d = 1 \text{ nA}$ decreases from 11 V to 7 V, evidencing the reduction of charge traps associated with vacancies in the WSe₂ sheets. Therefore, the improved transistor performance after thiophenol functionalization including the increased electron mobility and current density can be attributed to the elimination of trap states originated from Se vacancies and the n-type doping effect on WSe₂ channel. Control experiments were carried out after laser irradiation without molecular functionalization. It revealed that the laser irradiation generated more defects and decreased the drain current in the transfer curves. The following annealing

process did not recover the drain current (Figure S8), which shows the main function of thiophenol molecules in the defect passivation.

Figures 4c and 4d display the evolution of PL spectra at 77 K after laser irradiation and molecular functionalization. After 1 min laser irradiation, the defect-related peak X_b became broader and its spectra weight increased from 47% to 61%. After 6 min laser irradiation, another defect-related peak X_b' emerged and the spectra weight of defect-related peaks (X_b and X_b') further increased to 84%. After the thiophenol functionalization, the defect-related peaks have been greatly suppressed and the intensity of the PL peak originating from trion and exciton emissions increased by a factor of 10. The PL spectra at 300 K (inset of Figure 4c) also show a dramatic intensity enhancement after thiophenol adsorption. From the PL results, we confirm that laser irradiation can induce the desorption of absorbed molecules and the exposure/creation of chemically active defects in WSe_2 . Moreover, the thiophenol molecules can effectively passivate the defects, including the intrinsic defects and the created ones. Compared with PL spectra results in Figure 2d, the additional laser irradiation process contributes to a full passivation of defect-related peaks. The "ambient" molecules, i.e. oxygen and water molecules, can be adsorbed on the intrinsic vacancy sites in WSe_2 , inhibiting the exposure of chemically active vacancies to thiophenol molecules (Figure S9). The additional laser irradiation process can effectively desorb these adsorbents and promote the interaction of thiophenols with the vacancies.

We extended our study to the use of benzeneselenol molecules to passivate the defect in WSe_2 (Figure S10). After molecular functionalization, the drain current at $V_g = 80$ V dramatically increased from 8 nA to 276 nA. However, after the vacuum annealing, the drain current at $V_g = 80$ V decreased to 62 nA. Compared with thiophenol passivation, benzeneselenol molecules induce a stronger n-type doping effect on WSe_2 , which is consistent with our theoretical calculation results (Table S2). However, the thermal stability of benzeneselenol is much worse than that of thiophenol.^[30] The decomposition and the desorption of benzeneselenol molecules

greatly affected the interaction of molecules with Se vacancy sites. Therefore, we can conclude that thiolated molecules are more suitable to passivate defects and modulate the carrier density in WSe₂. Further studies (for example the exploration of molecular deposition conditions) can be conducted to enhance the selenol/vacancy interaction to enrich the molecular functionalization strategy on transition metal diselenides.

We further test the stability of thiophenol-passivated WSe₂ FET. The transfer curves in the thiophenol-passivated device displayed good drain current stability during the three days of storage in the glovebox (Figure S11). In comparison, the drain current in the transfer curves of the pristine device degraded after three days of storage. This is because the chemically active vacancy sites in the pristine device can be unintentionally doped by gas molecules in the surrounding environment. Therefore, thiophenol can effectively passivate the vacancy defects in WSe₂ and improve both the material stability and the device performance.

3. Conclusion

In summary, we have imaged by STM the intrinsic Se vacancies on the freshly exfoliated WSe₂ samples and showed the adsorption of thiophenol molecules at the chemically active Se vacancy sites for the first time. By studying the carrier transport in monolayer WSe₂ back-gate FETs and PL spectra of monolayer flake we demonstrated that thiophenol molecules are capable to passivate the defect states in WSe₂. The passivated monolayer WSe₂ FETs exhibit higher current density (an increase of I_d at $V_g = 90$ V by a factor of 100), improved electron mobility (from 0.015 to 0.79 cm²V⁻¹s⁻¹) and increased I_{on}/I_{off} ratio (from 1×10^4 to 1×10^6). A decrease in defect-related PL peak intensity also indicates the effective passivation of defects in monolayer WSe₂. Theoretical calculation provided unambiguous evidence for the formation of strong interaction between the thiol group of the molecules and Se vacancies in WSe₂ yielding n-type doping and the dynamic recovery of defect states originating from Se vacancies. Furthermore, the defect engineering in WSe₂ by laser irradiation enables to create more

chemically active defects, which can be effectively passivated by thiophenol molecules. Our molecular approach to engineer defects in WSe₂ flakes is a powerful strategy that can be extended to other transition metal diselenides, enabling functional diversity for high-performance TMD-based electronic devices

4. Experimental Section

Materials: Bulk WSe₂ crystals were purchased from commercial vendors (HQ graphene). The thiophenol (Product No. 240249) and benzeneselenol (Product No. 375152) were purchased from Sigma-Aldrich.

Molecular functionalization on WSe₂: The substrates holding WSe₂ FETs or monolayer flakes were fixed onto the lid of a 20 mL glass container filled with 100 μL of thiophenol. The lid was closed with the sample surface facing the liquid, and the container was saturated with molecular vapor by heating at 50 °C for 15 min. All the process was carried out under inert atmosphere (N₂-filled glovebox). Solvent molecules, especially oxygen-containing molecules (such as ethanol), have the chance to fill in the Se vacancy sites and inhibit the exposure of chemically active Se vacancies to thiol molecules. The vapor-phase deposition of thiol molecules under inert atmosphere can rule out the negative effect of solvent molecules.

Scanning tunnelling microscopy: STM measurements were carried out by using a Veeco scanning tunneling microscope (multimode Nanoscope III, Veeco) operating with a piezoelectric scanner. The substrates were glued onto a magnetic disk and an electric contact was made with (conductive) silver paint (Aldrich Chemicals). The STM tips were mechanically cut from a Pt/Ir wire (80%/20%, diameter 0.25 mm). The images were obtained at room temperature. The raw STM data were processed through the application of background flattening, and the drift of the piezo was corrected using the underlying WSe₂ lattice as a reference.

Photoluminescence spectroscopy characterization: The PL spectroscopy of monolayer WSe₂ were acquired with a Renishaw InVia spectrometer equipped with a 532 nm laser. Monolayer WSe₂ flakes were mechanically exfoliated from WSe₂ crystals onto SiO₂/Si substrate. The excitation power was kept below 1 mW to avoid the local heating and damaging effect. The Si Raman peak at 520.5 cm⁻¹ was used for normalization. Low-temperature PL spectra were characterized with the aid of Linkam T95 system controller in an inert (N₂) environment. Laser with a relatively high-power density 2.6×10^5 W/cm² was used to irradiate on the monolayer WSe₂ flake to expose and create defects.

Device fabrication and characterization: Monolayer WSe₂ flakes are mechanically exfoliated by the scotch tape-based method and transferred to the 270 nm SiO₂/Si substrate. Back-gated FETs were fabricated by e-beam lithography and the Au metal electrodes were thermally evaporated onto the patterned substrate. The lift-off process was carried out in warm acetone (50 °C) and the as-fabricated devices were annealed at 150 °C for 12 h in a high-vacuum chamber to desorb atmospheric adsorbates. All the devices were kept in a nitrogen-filled glovebox after annealing and electrically characterized in a probe station connected to a Keithley 2636. After the molecular functionalization, the second annealing process was conducted at 150 °C for 12 h in a high-vacuum chamber to desorb physisorbed molecules and improve the interaction between thiophenol molecules and vacancy sites.

The carrier mobility μ was determined by the following equation:

$$\mu = \frac{dI_d}{dV_g} \times \frac{L}{WC_iV_d}$$

where L and W are the channel length and width, and C_i is the capacitance per unit area.

The molecule-induced doping density was calculated by:

$$\Delta n = C_i \frac{\Delta V}{q}$$

where ΔV is the difference in the threshold voltage (V_{th}) before and after thiophenol functionalization.

Theoretical Calculation: DFT calculations were performed with the projector-augmented wave (PAW) basis set, as implemented in the VASP code.^[35, 36], with the exchange and correlation effects treated at the Perdew–Burke–Ernzerhof (PBE) level,^[37] incorporating dispersion forces by Grimme correction (PBE+D2),^[37, 38] and dipole moment correction along the ‘c’ axis (Z direction & perpendicular to the WSe₂ surface) with a kinetic energy cut-off of 600 eV and using a Monkhorst-Pack sampling of 3×3×1 for the Brillouin zone (BZ) integration on a 4×4×1 supercell of WSe₂ monolayer with the vacuum space set to be 30 Å to avoid the interaction with periodic images. Geometries of pristine and defective (−3% Se) WSe₂ surfaces, as well as the thiophenol adsorbed WSe₂ were fully optimized prior to calculation of work functions. The same computational criteria were used for calculations at the hybrid level of theory (HSE06) and also for *ab-initio* molecular dynamics simulations, which were performed at NVT ensemble for 120 ps - using the optimized geometries as initial configurations. Work function (ϕ) of all the systems was calculated as difference of Fermi energy (E_f , taken as the center of band gap) and the electrostatic potential at vacuum level (E_p). DDEC6 - bond order and overlap population analysis was performed using Chargemol program^[39-42].

Supporting Information

Supporting Information is available from the Wiley Online Library or from the author.

Acknowledgements

Yuda Zhao and Sai Manoj Gali contributed equally to this work. Y.Z. and P.S. conceived the experiment and designed the study. Y.Z. performed the PL, AFM, XPS characterization and carried out the device fabrication and characterization. C.W. carried out the STM study. S.M.G., A.P., and A.S. performed the quantum-chemical calculations. D.B. and S.M.G. supervised the theoretical work. Y.Z. wrote the paper. All authors discussed the results and contributed to the interpretation of data as well as to editing the manuscript.

Device fabrication was carried out in part at the nanotechnology facility eFab (IPCMS, Strasbourg). We acknowledge funding from European Commission through the ERC project SUPRA2DMAT (GA-833707), the Marie-Curie IEF STELLAR (GA-795615), the Graphene Flagship Core 3 project (GA-881603), the Agence Nationale de la Recherche through the Labex

projects CSC (ANR-10-LABX-0026 CSC) and NIE (ANR-11-LABX-0058 NIE) within the Investissement d'Avenir program (ANR-10-120 IDEX-0002-02), the International Center for Frontier Research in Chemistry (icFRC). The work in Mons is supported by the Belgian National Fund for Scientific Research (FRS-FNRS), within FNRS-PDR-TOREADOR project (T.0051.18). Computational resources were provided by the Consortium des Équipements de Calcul Intensif (CÉCI) funded by F.R.S.-FNRS under Grant F.R.S.-FNRS under the conventions N° 2.4.617.07.F and N° 2.5020.11. DB is FNRS Research Director.

Received: ((will be filled in by the editorial staff))

Revised: ((will be filled in by the editorial staff))

Published online: ((will be filled in by the editorial staff))

References

- [1] S. B. Desai, S. R. Madhvapathy, A. B. Sachid, J. P. Llinas, Q. Wang, G. H. Ahn, G. Pitner, M. J. Kim, J. Bokor, C. Hu, H.-S. P. Wong, A. Javey, *Science* **2016**, *354*, 99.
- [2] B. Radisavljevic, A. Radenovic, J. Brivio, V. Giacometti, A. Kis, *Nat. Nanotechnol.* **2011**, *6*, 147.
- [3] C. D. English, K. K. H. Smithe, R. L. Xu, E. Pop, "Approaching ballistic transport in monolayer MoS₂ transistors with self-aligned 10 nm top gates", presented at *2016 IEEE International Electron Devices Meeting (IEDM)*, 3-7 Dec. 2016.
- [4] S. Das, H.-Y. Chen, A. V. Penumatcha, J. Appenzeller, *Nano Lett.* **2013**, *13*, 100.
- [5] S.-L. Li, K. Tsukagoshi, E. Orgiu, P. Samorì, *Chem. Soc. Rev.* **2016**, *45*, 118.
- [6] Y. Zhao, K. Xu, F. Pan, C. Zhou, F. Zhou, Y. Chai, *Adv. Funct. Mater.* **2017**, *27*, 1603484.
- [7] L. Liu, Y. Lu, J. Guo, *IEEE Trans. Electron Devices* **2013**, *60*, 4133.
- [8] H. Fang, S. Chuang, T. C. Chang, K. Takei, T. Takahashi, A. Javey, *Nano Lett.* **2012**, *12*, 3788.
- [9] W. Liu, J. Kang, D. Sarkar, Y. Khatami, D. Jena, K. Banerjee, *Nano Lett.* **2013**, *13*, 1983.
- [10] M.-A. Stoeckel, M. Gobbi, T. Leydecker, Y. Wang, M. Eredia, S. Bonacchi, R. Verucchi, M. Timpel, M. V. Nardi, E. Orgiu, P. Samorì, *ACS Nano* **2019**, *13*, 11613.
- [11] W. Zhang, Z. Huang, W. Zhang, Y. Li, *Nano Res.* **2014**, *7*, 1731.
- [12] A. Allain, A. Kis, *ACS Nano* **2014**, *8*, 7180.
- [13] K. Kaasbjerg, K. S. Thygesen, K. W. Jacobsen, *Phys. Rev. B* **2012**, *85*, 115317.
- [14] B. Radisavljevic, A. Kis, *Nat. Mater.* **2013**, *12*, 815.
- [15] Z. Wu, Z. Luo, Y. Shen, W. Zhao, W. Wang, H. Nan, X. Guo, L. Sun, X. Wang, Y. You, Z. Ni, *Nano Res.* **2016**, *9*, 3622.
- [16] C.-P. Lu, G. Li, J. Mao, L.-M. Wang, E. Y. Andrei, *Nano Lett.* **2014**, *14*, 4628.
- [17] D. Liu, Y. Guo, L. Fang, J. Robertson, *Appl. Phys. Lett.* **2013**, *103*, 183113.
- [18] H.-P. Komsa, J. Kotakoski, S. Kurasch, O. Lehtinen, U. Kaiser, A. V. Krasheninnikov, *Phys. Rev. Lett.* **2012**, *109*, 035503.
- [19] J. Hong, Z. Hu, M. Probert, K. Li, D. Lv, X. Yang, L. Gu, N. Mao, Q. Feng, L. Xie, J. Zhang, D. Wu, Z. Zhang, C. Jin, W. Ji, X. Zhang, J. Yuan, Z. Zhang, *Nat. Commun.* **2015**, *6*, 6293.
- [20] S. Roy, W. Choi, S. Jeon, D.-H. Kim, H. Kim, S. J. Yun, Y. Lee, J. Lee, Y.-M. Kim, J. Kim, *Nano Lett.* **2018**, *18*, 4523.
- [21] H. Qiu, T. Xu, Z. Wang, W. Ren, H. Nan, Z. Ni, Q. Chen, S. Yuan, F. Miao, F. Song, G. Long, Y. Shi, L. Sun, J. Wang, X. Wang, *Nat. Commun.* **2013**, *4*, 2642.
- [22] S. G. McAdams, E. A. Lewis, J. R. Brent, S. J. Haigh, A. G. Thomas, P. O'Brien, F. Tuna, D. J. Lewis, *Adv. Funct. Mater.* **2017**, *27*, 1703646.

- [23] E. P. Nguyen, B. J. Carey, J. Z. Ou, J. van Embden, E. D. Gaspera, A. F. Chrimes, M. J. S. Spencer, S. Zhuiykov, K. Kalantar-zadeh, T. Daeneke, *Adv. Mater.* **2015**, *27*, 6225.
- [24] Z. Yu, Z.-Y. Ong, Y. Pan, Y. Cui, R. Xin, Y. Shi, B. Wang, Y. Wu, T. Chen, Y.-W. Zhang, G. Zhang, X. Wang, *Adv. Mater.* **2016**, *28*, 547.
- [25] Z. Yu, Y. Pan, Y. Shen, Z. Wang, Z.-Y. Ong, T. Xu, R. Xin, L. Pan, B. Wang, L. Sun, J. Wang, G. Zhang, Y. W. Zhang, Y. Shi, X. Wang, *Nat. Commun.* **2014**, *5*, 5290.
- [26] K. Cho, M. Min, T.-Y. Kim, H. Jeong, J. Pak, J.-K. Kim, J. Jang, S. J. Yun, Y. H. Lee, W.-K. Hong, T. Lee, *ACS Nano* **2015**, *9*, 8044.
- [27] M. Amani, D.-H. Lien, D. Kiriya, J. Xiao, A. Azcatl, J. Noh, S. R. Madhvapathy, R. Addou, S. KC, M. Dubey, K. Cho, R. M. Wallace, S.-C. Lee, J.-H. He, J. W. Ager, X. Zhang, E. Yablonovitch, A. Javey, *Science* **2015**, *350*, 1065.
- [28] Y. J. Zheng, Y. Chen, Y. L. Huang, P. K. Gogoi, M.-Y. Li, L.-J. Li, P. E. Trevisanutto, Q. Wang, S. J. Pennycook, A. T. S. Wee, S. Y. Quek, *ACS Nano* **2019**, *13*, 6050.
- [29] C. Zhang, C. Wang, F. Yang, J.-K. Huang, L.-J. Li, W. Yao, W. Ji, C.-K. Shih, *ACS Nano* **2019**, *13*, 1595.
- [30] F. P. Cometto, E. M. Patrino, P. Paredes Olivera, G. Zampieri, H. Ascolani, *Langmuir* **2012**, *28*, 13624.
- [31] S. Bertolazzi, M. Gobbi, Y. Zhao, C. Backes, P. Samorì, *Chem. Soc. Rev.* **2018**, *47*, 6845.
- [32] Z. Wu, W. Zhao, J. Jiang, T. Zheng, Y. You, J. Lu, Z. Ni, *J. Phys. Chem. C* **2017**, *121*, 12294.
- [33] A. M. Jones, H. Yu, N. J. Ghimire, S. Wu, G. Aivazian, J. S. Ross, B. Zhao, J. Yan, D. G. Mandrus, D. Xiao, W. Yao, X. Xu, *Nat. Nanotechnol.* **2013**, *8*, 634.
- [34] Z. He, X. Wang, W. Xu, Y. Zhou, Y. Sheng, Y. Rong, J. M. Smith, J. H. Warner, *ACS Nano* **2016**, *10*, 5847.
- [35] G. Kresse, J. Furthmüller, *Phys. Rev. B* **1996**, *54*, 11169.
- [36] G. Kresse, D. Joubert, *Phys. Rev. B* **1999**, *59*, 1758.
- [37] J. P. Perdew, K. Burke, M. Ernzerhof, *Phys. Rev. Lett.* **1996**, *77*, 3865.
- [38] S. Grimme, *J. Comput. Chem.* **2006**, *27*, 1787.
- [39] T. A. Manz, N. G. Limas, *RSC Adv.* **2016**, *6*, 47771.
- [40] N. G. Limas, T. A. Manz, *RSC Adv.* **2016**, *6*, 45727.
- [41] T. A. Manz, *RSC Adv.* **2017**, *7*, 45552.
- [42] T. A. Manz, N. Gabaldon Limas, **2017**, ddec.sourceforge.net.

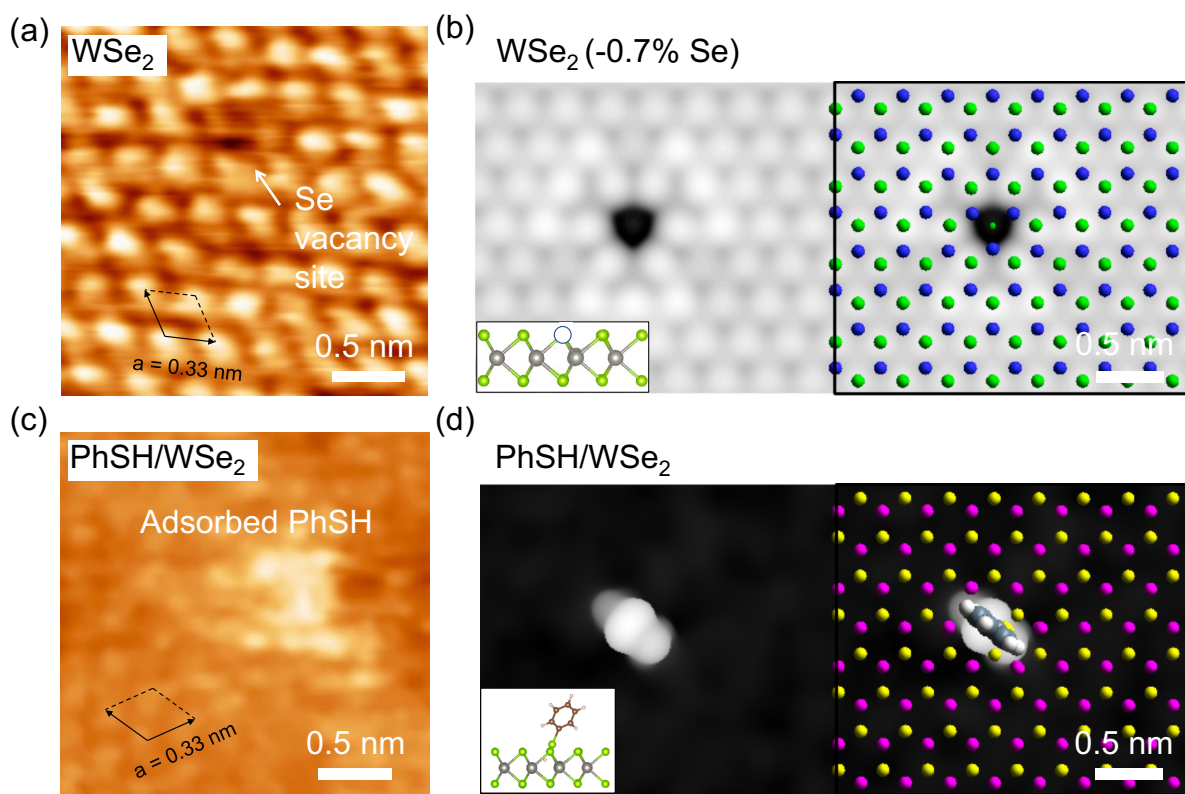


Figure 1. (a) Experimental scanning tunneling microscopic (STM) height image of the freshly exfoliated WSe_2 surface, showing the Se vacancy site. Tunneling parameters: tip bias voltage (V_t) = -850 mV, average tunneling current (I_t) = 22 pA. (b) Simulated STM image of WSe_2 with 0.7% Se vacancy. Inset shows the schematic drawing of crystal structure of WSe_2 containing a Se vacancy in the side-view. (c) Experimental STM height image of WSe_2 surface with the adsorption of thiophenol molecules. $V_t = -800$ mV, $I_t = 10$ pA. (d) Simulated STM image of WSe_2 (-0.7% Se) with the vertical adsorption of thiophenol molecules at the Se vacancy site. Inset shows the schematic drawing of crystal structure of WSe_2 with the adsorption of thiophenol molecules at the Se vacancy site in the side-view.

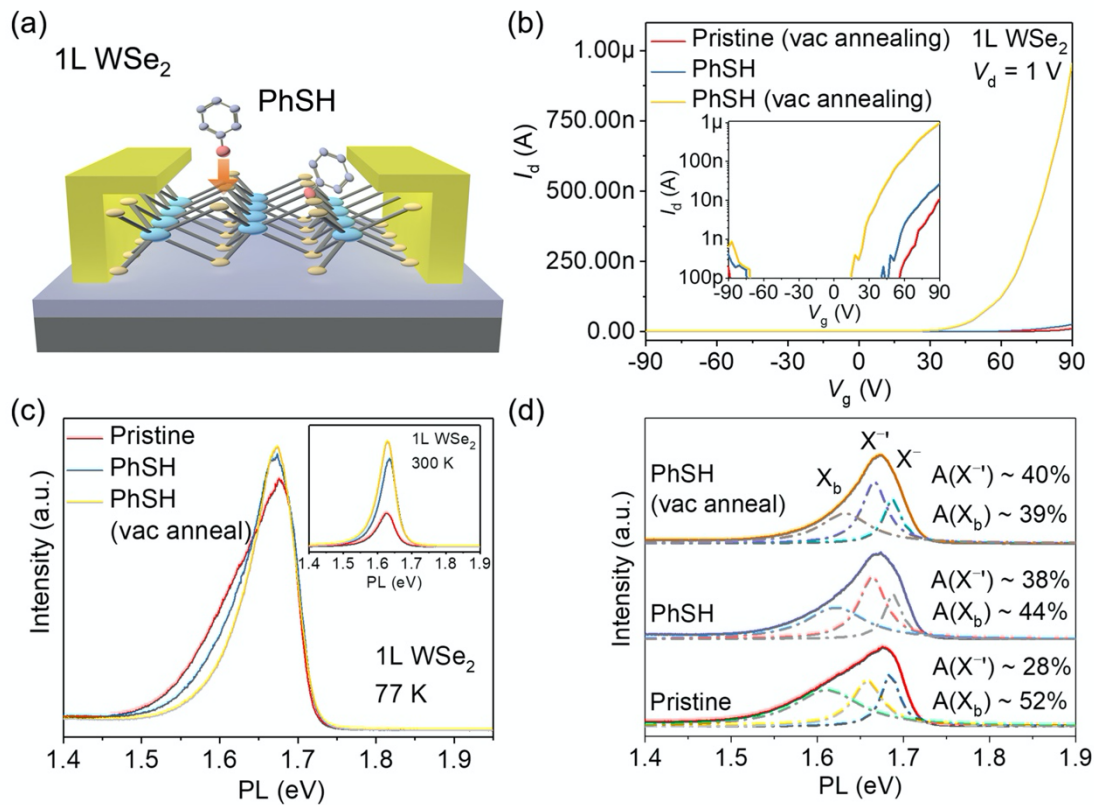


Figure 2. (a) Schematic of back-gated monolayer WSe₂ field-effect transistor (FET) with the adsorption of thiophenol molecules. (b) Transfer characteristics in lin-lin scale of a pristine monolayer WSe₂ FET before (red line) and after (blue line) exposure to thiophenol vapors, and after vacuum annealing (yellow line). The curves are also shown in log–lin scale in the inset. (c) Photoluminescence (PL) spectra of a pristine monolayer WSe₂ flake measured at 77 K before (red line) and after (blue line) exposure to thiophenol vapors, and after vacuum annealing (yellow line). Inset shows PL spectra measured at 300 K. (d) The PL spectra at 77 K were fitted with a Lorentzian function to take into account the defect-mediated emission occurring at $X_b \approx 1.61$ eV and two negatively charged trion peaks at $X^- \approx 1.68$ eV and $X'^- \approx 1.66$ eV.

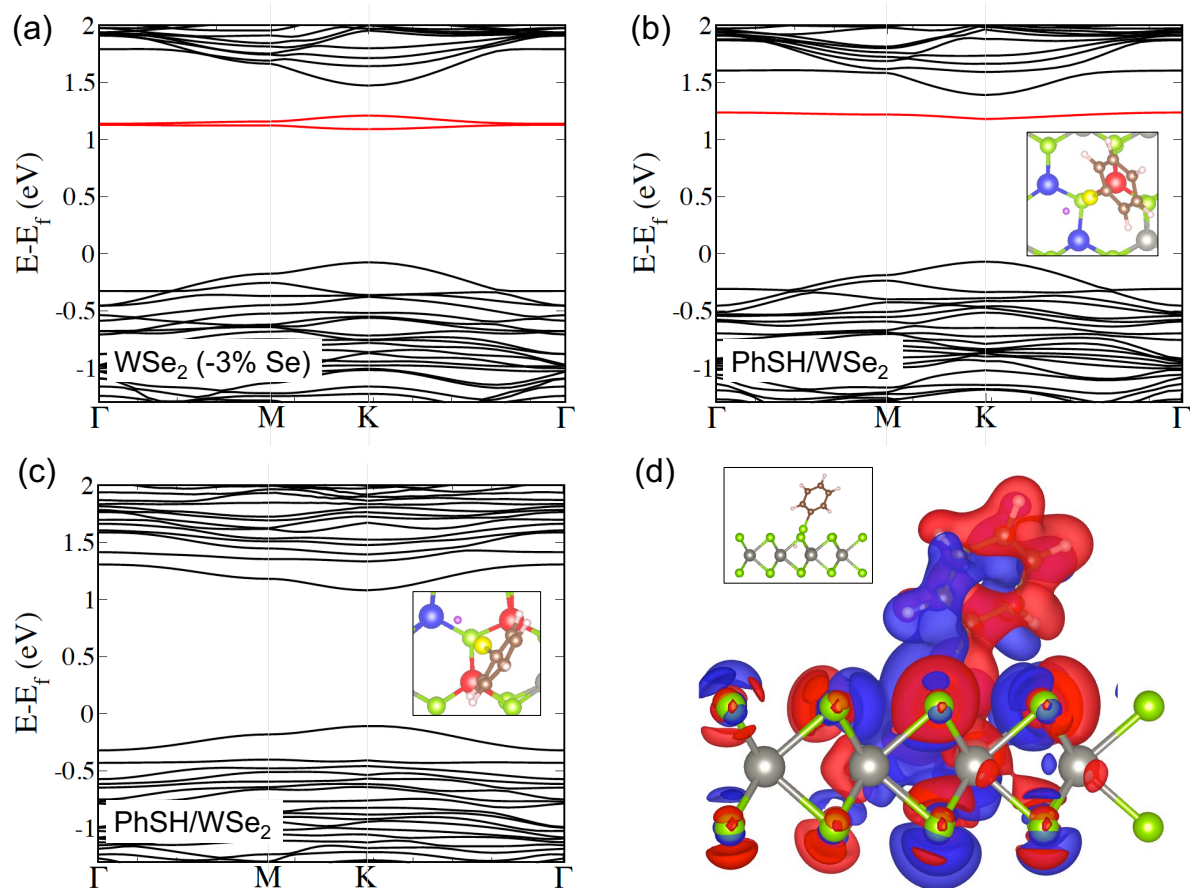


Figure 3. Electronic band structure of monolayer WSe₂ (a) with 3% Se vacancies and with the adsorption of thiophenol on Se vacancy sites when (b) sulfur (hydrogen) atom is interacting with one (two) neighboring tungsten atom(s) and (c) sulfur (hydrogen) atom is interacting with two (one) neighboring tungsten atom(s); Insets in (b) and (c) represent the atomic configuration with tungsten atom(s) close to sulfur (hydrogen) atom(s) highlighted in red (blue) color. The midgap defect states below CBM are indicated in red color. (d) Charge density difference plot of WSe₂ with the adsorption of thiophenol on Se vacancy sites.

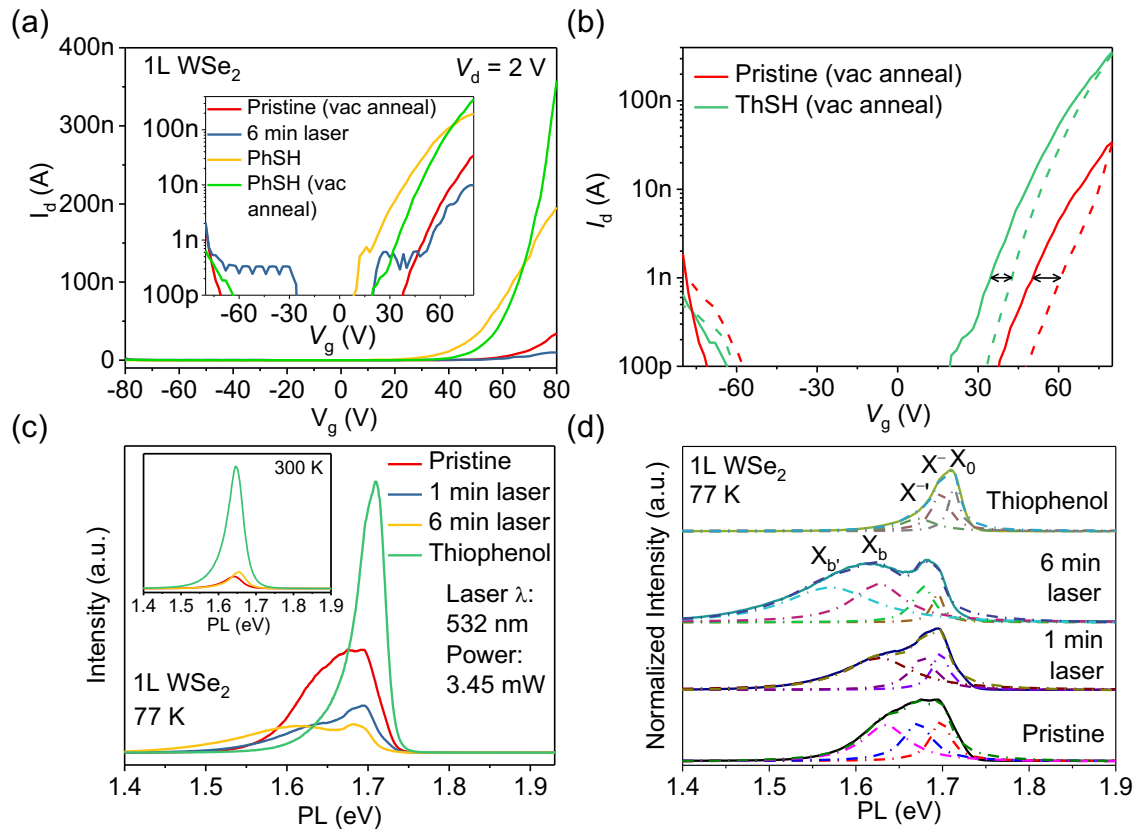


Figure 4. Transfer characteristics in lin-lin scale of a pristine monolayer WSe₂ FET before (red line) and after (blue line) laser irradiation, after exposure to thiophenol vapors (yellow line), and after vacuum annealing (green line). The curves are also shown in log–lin scale in the inset. (b) Transfer curves in solid lines are acquired with the sweep direction from –80 to +80 V and the dashed lines correspond to the opposite sweep direction, showing the device hysteresis. (c) Photoluminescence (PL) spectra measured at 77 K of a pristine monolayer WSe₂ flake (red line), after one-minute laser irradiation (blue curve), after six-minute laser irradiation (yellow line), and after exposure to thiophenol vapors (green line). Inset shows the PL spectra at 300 K. (d) The PL spectra at 77 K were fitted with a Lorentzian function to take into account the defect-mediated emissions, negatively charged trion peaks and neutral exciton peak.